iScience

CellPress
OPEN ACCESS

Article

Enzymatic activity of glycosyltransferase GLT8D1 promotes human glioblastoma cell migration

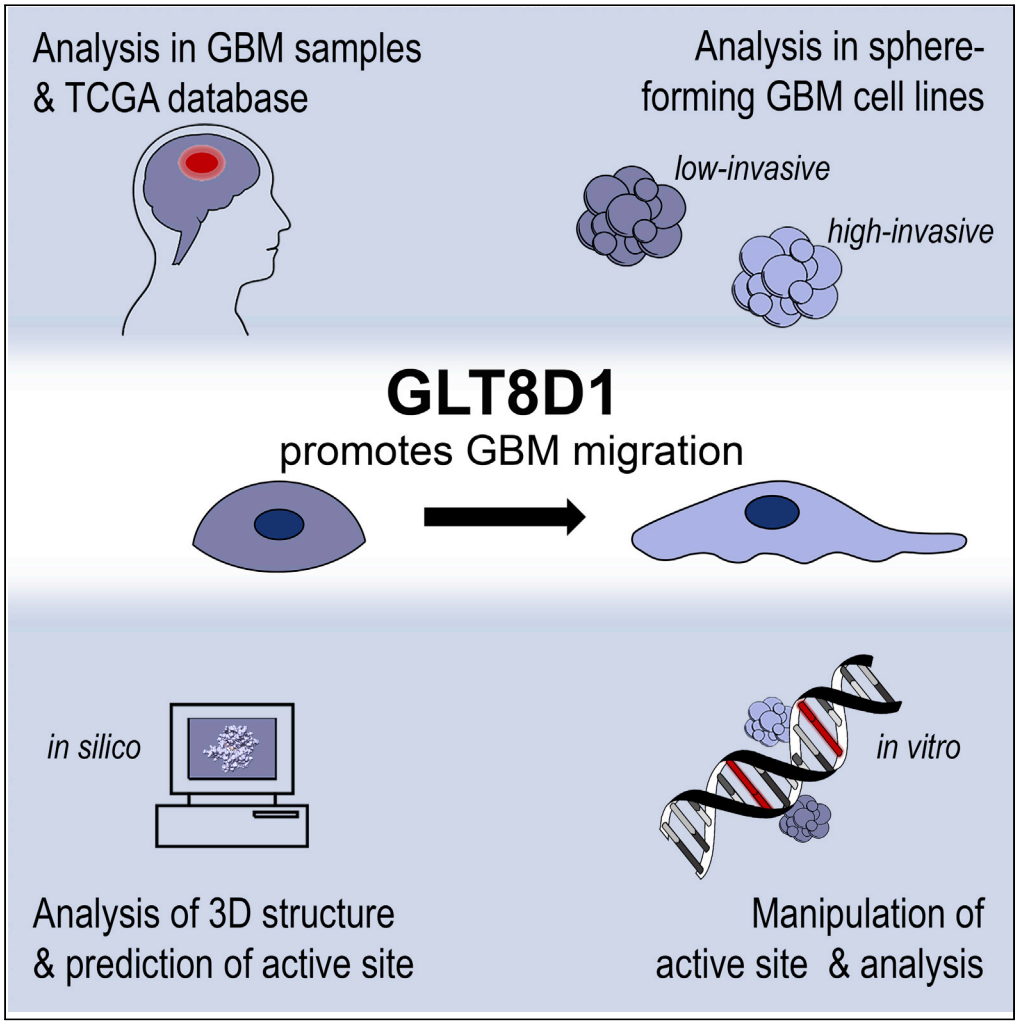

Elena I. Ilina, Camille Cialini, Dietlind L. Gerloff, ..., Simone P. Niclou, Tanja Müller, Michel Mittelbronn

michel.mittelbronn@lih.lu (M.M.)
tanja.mueller@lih.lu (T.M.)

Highlights

The glycosyltransferase GLT8D1 is enriched in GBM tissue and cells

In silico analysis predicts the 3D structure and the active site of GLT8D1

Enzymatically active GLT8D1 promotes GBM migration

Manipulation of GLT8D1 enzymatic activity decreases GBM migration

Ilina et al., iScience *25*, 103842
February 18, 2022
https://doi.org/10.1016/j.isci.2022.103842

iScience

CellPress
OPEN ACCESS

Article

Enzymatic activity of glycosyltransferase GLT8D1 promotes human glioblastoma cell migration

Elena I. Ilina,[1,2] Camille Cialini,[1,2] Dietlind L. Gerloff,[3] Maitane Duarte Garcia-Escudero,[1,2] Céline Jeanty,[4] Marie-Laëtitia Thézénas,[4] Antoine Lesur,[4] Vincent Puard,[4] François Bernardin,[4] Alina Moter,[1,2] Anne Schuster,[1,5] Monika Dieterle,[1,5] Anna Golebiewska,[1,5] Jean-Jacques Gérardy,[2,6] Gunnar Dittmar,[4,7] Simone P. Niclou,[1,5] Tanja Müller,[1,2,10,*] and Michel Mittelbronn[1,2,6,7,8,9,10,11,*]

SUMMARY

Glioblastoma (GBM) is the most aggressive primary brain tumor characterized by infiltrative growth of malignant glioma cells into the surrounding brain parenchyma. In this study, our analysis of GBM patient cohorts revealed a significantly higher expression of *Glycosyltransferase* 8 *domain containing 1* (*GLT8D1*) compared to normal brain tissue and could be associated with impaired patient survival. Increased *in vitro* expression of *GLT8D1* significantly enhanced migration of two different sphere-forming GBM cell lines. By *in silico* analysis we predicted the 3D-structure as well as the active site residues of GLT8D1. The introduction of point mutations in the predicted active site reduced its glycosyltransferase activity *in vitro* and consequently impaired GBM tumor cell migration. Examination of GLT8D1 interaction partners by LC-MS/MS implied proteins associated with cytoskeleton and intracellular transport as potential substrates. In conclusion, we demonstrated that the enzymatic activity of glycosyltransferase GLT8D1 promotes GBM cell migration.

INTRODUCTION

Glioblastoma (GBM) is the most aggressive primary brain tumor characterized by diffuse infiltration of malignant glioma cells into the surrounding brain parenchyma. This hallmark is one of the major obstacles in GBM treatment, as it impedes complete surgical resection (Vollmann-Zwerenz et al., 2020). Among multiple dysregulated intracellular processes driving GBM tumorigenesis, posttranslational protein modifications (PTM) are frequently altered (Lemjabbar-Alaoui et al., 2015). Co-translational and posttranslational modifications of newly synthesized proteins are necessary for their functional activation with glycosylation representing the most frequent modification associated with malignancy (Vajaria et al., 2018). Examination of *Glycosyltransferase* 8 *domain containing 1* (*GLT8D1*) expression levels using the Cancer Genome Atlas (TCGA) patient dataset within the GlioVis platform revealed enhanced expression levels of this glycosyltransferase enzyme in GBM tissue (Figure 1A). However, only little is known about the physiological and pathological functions of this gene and its corresponding protein, to date.

Several studies linked GLT8D1 dysfunction to neurodegenerative or neurological diseases, such as amyotrophic lateral sclerosis (ALS) or schizophrenia (Sasayama et al., 2014; Yang et al., 2018; Moll et al., 2019; Cooper-Knock et al., 2019; Brenner and Weishaupt, 2019). Although no association between GLT8D1 and the development of brain tumors was described so far, there is first evidence of a tumorigenic role of this protein in other cancer entities, such as head and neck squamous cell carcinomas (HNSCCs) and melanomas, both being highly invasive and metastatic, respectively (Hwang et al., 2013; Hu et al., 2019).

In the present study, we showed for the first time that the glycosyltransferase GLT8D1 is involved in GBM pathogenesis and is tightly linked to regulation of glioma cell migration. By combining *in silico* and *in vitro* approaches with analysis of clinical samples, we could elucidate possible functions of GLT8D1 in GBM. Bioinformatic analysis of GLT8D1 homologs implied an enzymatic function with glycosyltransferase activity. Whereas wild-type GLT8D1 was triggering GBM cell migration, contributing to the diffuse infiltration of the tumor cells, partial loss of enzymatic function was sufficient to abolish the pro-migratory

[1]Department of Cancer Research (DoCR), Luxembourg Institute of Health (LIH), 1526 Luxembourg, Luxembourg

[2]Luxembourg Centre of Neuropathology (LCNP), 1526 Luxembourg, Luxembourg

[3]Foundation for Applied Molecular Evolution (FfAME), Alachua, FL 32615, USA

[4]Quantitative Biology Unit, Luxembourg Institute of Health (LIH), 1526 Luxembourg, Luxembourg

[5]NORLUX Neuro-Oncology Laboratory, Department of Cancer Research (DoCR), Luxembourg Institute of Health (LIH), 1526 Luxembourg, Luxembourg

[6]National Center of Pathology (NCP), Laboratoire National de Santé (LNS), 3555 Dudelange, Luxembourg

[7]Department of Life Sciences and Medicine (DLSM), University of Luxembourg, 4365 Esch sur Alzette, Luxembourg

[8]Luxembourg Centre for Systems Biomedicine (LCSB), University of Luxembourg, 4365 Esch-sur-Alzette, Luxembourg

[9]Faculty of Science, Technology and Medicine, University of Luxembourg, 4365 Esch-sur-Alzette, Luxembourg

[10]These authors contributed equally

[11]Lead contact

*Correspondence: michel.mittelbronn@lih.lu (M.M.), tanja.mueller@lih.lu (T.M.)

https://doi.org/10.1016/j.isci.2022.103842

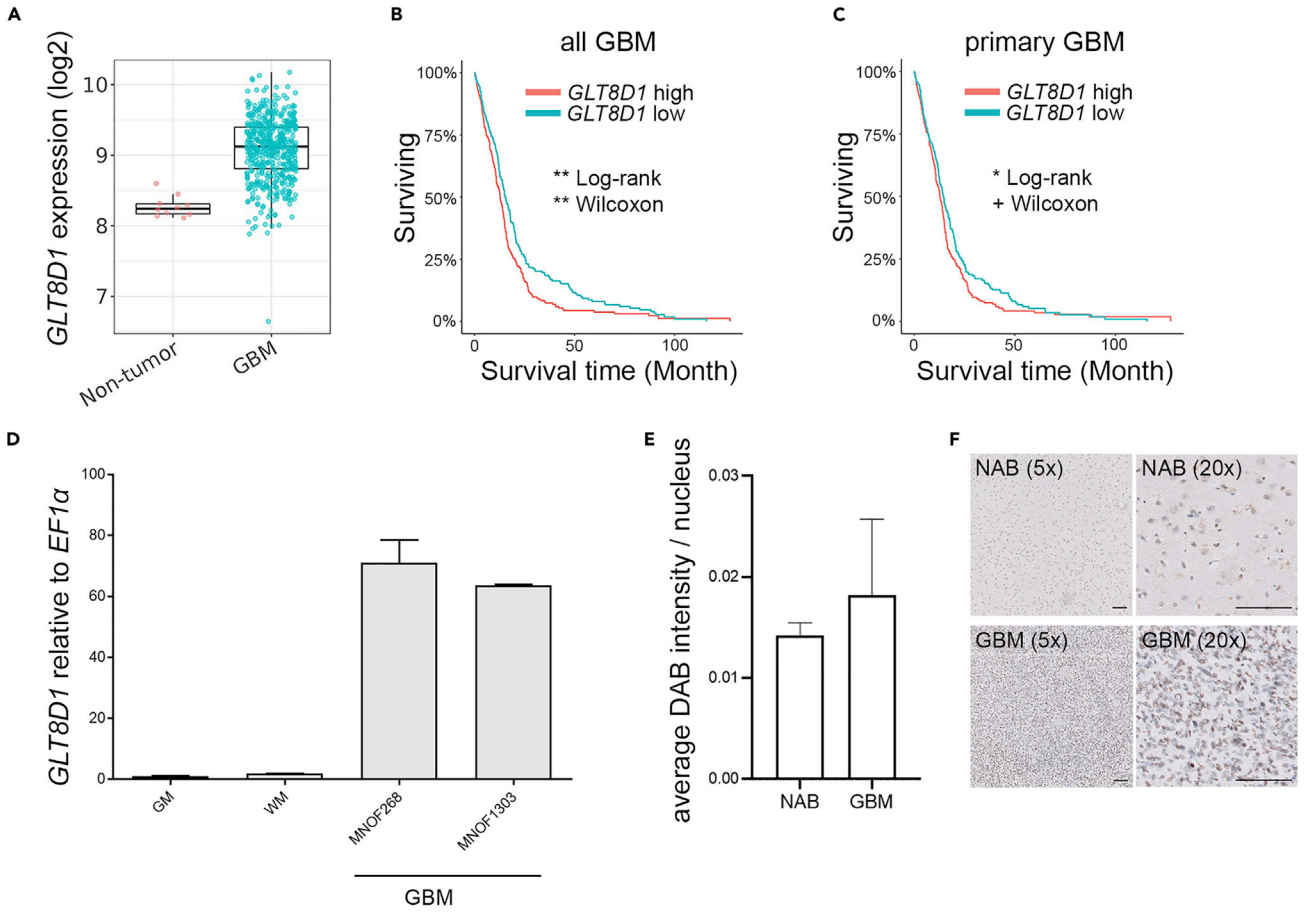

Figure 1. GLT8D1 gene expression and protein expression in clinical GBM samples

(A) *GLT8D1* mRNA expression in non-tumor vs. GBM samples (GlioVis platform, The Cancer Genome Atlas (TCGA_GBM) dataset, HG-U133A platform, total 538 entries). n = 10, median 8.24, mean 8.27, SD 0.15 (non-tumor), n = 528, median 9.12, mean 9.08, SD 0.43 (GBM), Tukey's Honest Significant Difference (HSD), ***p < 0.001.

(B) Kaplan-Meier survival analysis of the patients with the GBM (both primary and secondary tumors) showing low vs. high expression of *GLT8D1* (GlioVis platform, TCGA_GBM dataset, HG-U133A platform, total 538 entries). Median cutoff; n = 266 for *GLT8D1* high, n = 259 for *GLT8D1* low; Log rank **p = 0.0015; Wilcoxon **p = 0.0026.

(C) Kaplan-Meier survival analysis of the patients with the GBM (primary tumors only) showing low vs. high expression of *GLT8D1* (GlioVis platform, TCGA_GBM dataset, HG-U133A platform, total 538 entries). Median cutoff; n = 247 for *GLT8D1* high, n = 250 for *GLT8D1* low; Log rank *p = 0.0395; Wilcoxon p = 0.0524.

(D) *GLT8D1* expression in the cryo-preserved specimens of normal appearing brain (GM – gray matter, WM – white matter) vs. GBM WHO grade IV (qPCR). Mean of three technical replicates per sample + SEM is shown.

(E and F) Semiquantitative analysis of GLT8D1 protein expression determined on immunohistochemistry staining of FFPE sections from patient-derived normal appearing brain (NAB; n = 4) and GBM WHO grade IV specimens (GBM; n = 9). Analyzed was the average DAB intensity per nucleus. Data are represented as mean + SEM (F) Representative immunohistochemical DAB staining of GLT8D1 in the FFPE sections of the normal appearing brain (NAB) and of the GBM WHO grade IV specimen in two magnifications (scale bar 100μm).

phenotype of the tumor cells *in vitro*. Although further experimental analysis is required to decipher potential downstream targets, our findings propose a new target in GBM research with potential therapeutic implications.

RESULTS

GLT8D1 shows elevated expression in patient GBM tumor samples

To examine the relevance of *GLT8D1* in GBM pathology, RNA expression levels in human GBM samples as well as patients' survival data were evaluated using the GlioVis platform, TCGA dataset (http://gliovis.bioinfo.cnio.es, last accessed on the 11.07.2021; Bowman et al., 2017, STAR Methods). *GLT8D1* mRNA was elevated in GBM samples, as compared to the normal brain (Figure 1A). Kaplan-Mayer analysis

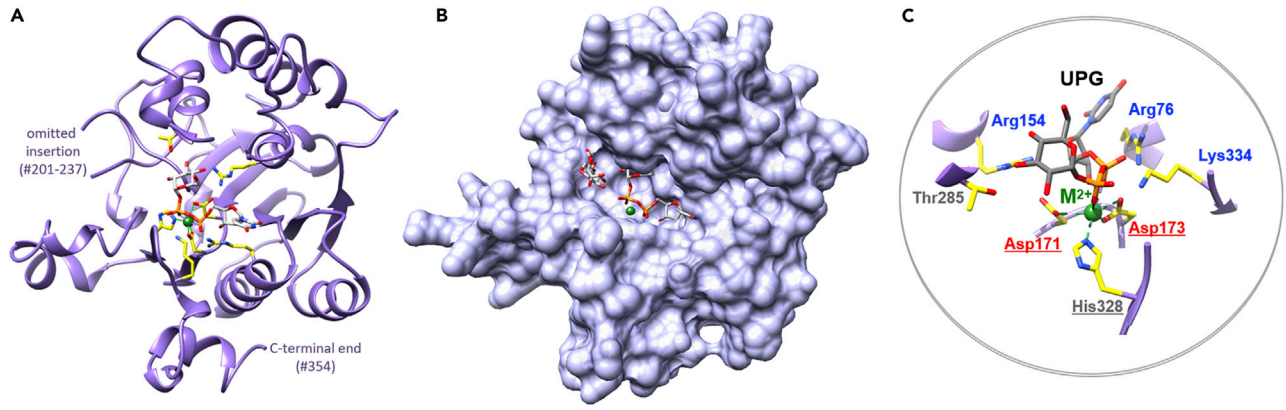

Figure 2. Predicted UDP-hexosyltransferase active site in GLT8D1

(A) Predicted active site in the homology-based 3D-model of GLT8D1 (residues 62-354).

(B) Location of the plausible substrate groove in the model based on UPG and substrate placeholder molecules.

(C) Approximate orientation of the predicted active site residues in a close-up, DxD centered view with UPG and metal ion (M^{2+}) locations (colored sticks/sphere). Label colors reflect positive (blue), negative (red), neutral (gray) charge at physiological pH, metal-coordinating residues are underlined. See also Figure S1 and Table S4.

displayed a more favorable survival prognosis for lower *GLT8D1* expression in all GBMs (Figure 1B) and primary GBMs, specifically (Figure 1C). GLT8D1 mRNA-levels and protein levels were analyzed in normal-appearing brain tissue as well as in GBM tissue. Although *GLT8D1* mRNA was considerably elevated in GBM (Figure 1D), protein expression appeared very heterogeneous between the tumor samples (Figure 1E).

In silico analysis of GLT8D1 protein structure reveals putative enzymatic domain and characteristics

GLT8D1 is a member of the glycosyltransferase protein family 8 (GT8) (Cantarel et al., 2009). The approximately 42kDa GLT8D1 protein is expressed and highly conserved across animal species (Figure S1). It bears more distant relatedness also to the plant and protist kingdom members of GT8 but those may not be orthologs. All closest homologs of GLT8D1, orthologs as well as paralogs, are assigned to a distinct clade (clade 9) within the GT8 family (Taujale et al., 2020) to which a retaining glycosyl transfer mechanism is attributed (from, *a priori*, a UDP-hexosyl donor with unknown sugar specificity to an unknown acceptor substrate). Sequence conservation and properties allow to postulate a cytoplasmic amino terminus (residues 1-7 in UniProtKB: GL8D1_HUMAN), followed by a single-pass transmembrane region (TM; a. a. residues 8–28) and a lumenal/cytoplasmic domain (LU; a. a. residues 29–371) (Figures 3A and S1).

No 3D-protein structure of GLT8D1 has been determined experimentally to date, therefore models of the core of its LU domain were built for this study based on suitable template structures within the GT8 family (PDB: 3qvb, 4wma) and on alignments/patterns within the wider GT-A superfamily of glycosyltransferases (Figure 2; STAR Methods). Based on conservation and confident modeling of the active site region, catalytic activity of GLT8D1 can be strongly assumed. Key amino acid residues for such enzymatic function were identified and primarily include the highly conserved coordination site for the characteristic divalent metal ion (M^{2+}) (in GLT8D1: the 171-DDD-173 motif and H328) as well as putative contributors to UDP-hexose binding and/or active site stabilization (R76, R154, T285, and K334) (Figures 2A–2C and Table 1).

GLT8D1 is expressed and localized to the Golgi apparatus and endoplasmic reticulum in GBM cells

To further analyze the effect of GLT8D1 on GBM pathogenesis we examined its expression in two different GBM sphere-forming cell lines (NCH601 and NCH644). GLT8D1 mRNA and protein levels were significantly elevated in highly invasive NCH601 GBM cells compared to NCH644 owing a low-invasive phenotype (Figures 3A and 3B; Bougnaud et al., 2016). This leads us to the assumption that GLT8D1 may promote glioma cell migration. The presence of a TM domain in the GLT8D1 protein implies a putative association with

Table 1. Predicted UDP-hexosyltransferase active site in GLT8D1

GLT8D1 residue	Catalytic role	Prediction confidence	Notes
D171	M^{2+} coordination (Mn^{2+})	Evident	DxD motif, widely conserved in this role throughout the superfamily (GT-A)
D173	M^{2+} coordination (Mn^{2+})	Evident	DxD motif, widely conserved in this role throughout the superfamily (GT-A)
H328	M^{2+} coordination (Mn^{2+})	Evident	Widely conserved in this role throughout the superfamily (GT-A)
R76	Salt bridge to D172 (active site stabilization) and/or UDP binding (P)	Confident	Indicated by model structure, active site geometry, and sequence conservation
R154	UDP binding (P)	Confident	Indicated by model structure, active site geometry, and sequence conservation
K334	UDP binding (P)	Confident	Indicated by model structure, active site geometry, and sequence conservation
T285	UDP-Hexose binding/specificity	Probable	Predicted by model structure (conserved UDP-hexose orientation) and sequence conservation; substitution within xED motif (xDQ in most GT8)

Residues in this list are inferred to contribute to catalysis based on *in silico* analysis of homologous sequences and structures within the GT8 protein family. See alsoFigures 2 and S1 and Table S4.

organelle membranes. In contrast to the human protein atlas (as accessed on the 19.04.2020; https://www.proteinatlas.org/ENSG00000016864-GLT8D1/cell) but in line with the latest published data (Cooper-Knock et al., 2019), GLT8D1 was found to localize to the Golgi network as it was detected in both the cytoplasmic and Golgi-enriched fractions upon subcellular fractionation (Figure S2A). Furthermore, proximity ligation assays revealed GLT8D1 as localized to the Golgi apparatus and endoplasmic reticulum (ER) but absent in mitochondria, peroxisomes, or lysosomes (Figures 3C and S2B).

GLT8D1 overexpression promotes *in vitro* GBM cell migration

To investigate the impact of GLT8D1 on migration properties of GBM cells, wild type protein was ectopically overexpressed in the low-invasive NCH644 cells (Figures 3D and S3A) followed by the assessment of migration using the Boyden chamber assay. After 48h, migration of *GLT8D1* overexpressing cells was significantly increased as compared to control cells (Figures 3E, 3F, S3B, and S3C), whereas no effects on cell proliferation could be observed (Figure S3D). GLT8D1 knockdown lines were generated by stable expression of *GLT8D1*-targeting shRNA in the high-invasive NCH601 cells (Figures 3G and S3E). A significant reduction of cell migration through the Boyden chamber assay became evident already after 24h (Figures S3F and S3G) and was persistent after 48h (Figures 3H and 3I). Similar to the GLT8D1-overexpressing cells, no effects on proliferation could be observed in the knockdown experiments (Figure S3H).

HA-tagged GLT8D1 was introduced in the high-invasive NCH601 cells, stably expressing *GLT8D1* shRNA targeting the 3′-UTR region of the transcript (sh-GLT8D1 #2). This led to the ectopic overexpression of different GLT8D1 variants but knockdown of the endogenous protein (Figure 3J, here and further depicted as "sh-GLT8D1 + rescue"). Examination of the impact of protein re-expression on transwell migration in the Boyden chamber assay showed that re-expression of GLT8D1 restores the migration capacity of the NCH601 cells (Figures 3K, 3L, S3I, and S3J), whereas tumor cell proliferation remains unaffected (Figure S3K).

GLT8D1 possesses enzymatic activity *in vitro* and mutations within its active site diminish its pro-migratory properties

To shed light on the question if and how the structural and/or enzymatic domains of GLT8D1 are involved in modulating GBM cell migration, we designed several mutated proteins (Figures 4A and S4A). Wild type GLT8D1 consists of cytosolic-, TM-, and LU domains. The latter includes its putative glycosyltransferase active site with predicted metal ion-coordinating residues as well as residues with other roles (see above, Table 1). Two GLT8D1 overexpression constructs were generated, where metal ion binding would be affected through mutations in the metal-coordinating DxD-motif (DDD in GLT8D1): 171-ASD-173 (mAS1)

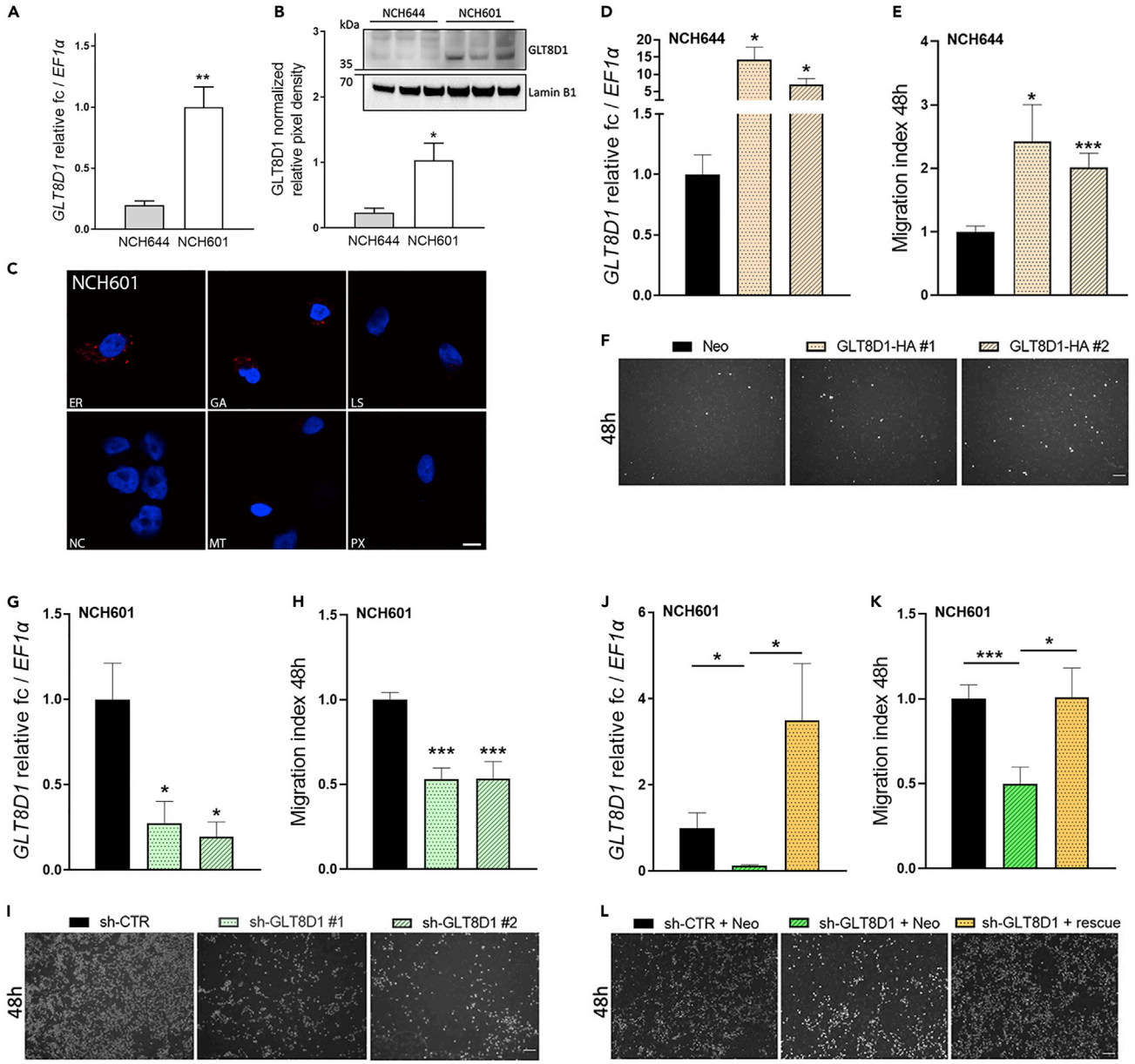

Figure 3. Impact of GLT8D1 expression on GBM cell migration

(A) *GLT8D1* expression in NCH644 and NCH601 cells (qPCR). Unpaired t-test, mean + SEM, n = 3 (**p = 0.0090).

(B) Representative immunoblot of GLT8D1 staining in the cell extracts of NCH644 and NCH601 cells and densitometric analysis. Unpaired t-test, mean + SEM, n = 3 (*p = 0.0434).

(C) Immunofluorescence images of GLT8D1 localization in the NCH601 cells as detected by proximity ligation assay. The red immunosignal indicates the interaction of GLT8D1 with the organelle-specific proteins. ER – endoplasmic reticulum (PDI), GA – Golgi apparatus (Golgin97), LS – lysosomes (LAMP1), MT – mitochondria (MTC02), PX – peroxisomes (Catalase). NC – negative control. Scale bar 10μm.

(D) *GLT8D1* expression in the GLT8D1-overexpressing NCH644 cells (qPCR). ANOVA, mean + SEM, n = 3 (*p = 0.0204 for GLT8D1-HA #1; *p = 0.0192 for GLT8D1-HA #2).

(E) Quantitative analysis of cell migration in the GLT8D1-overexpressing NCH644 cells after 48h (Boyden chamber assay). ANOVA, mean + SEM, n = 6 (*p = 0.0204 for GLT8D1-HA #1; ***p = 0.0004 for GLT8D1-HA #2).

(F) Representative images of the migrated GLT8D1-overexpressing NCH644 cells after 48h (Boyden chamber assay). Scale bar 100μm.

(G) *GLT8D1* expression in the GLT8D1-knockdown NCH601 cells (qPCR). ANOVA, mean + SEM, n = 4 (*p = 0.0265 for sh-GLT8D1 #1; *p = 0.0127 for sh-GLT8D1 #2).

(H) Quantitative analysis of the cell migration in the GLT8D1-knockdown NCH601 cells after 48h (Boyden chamber assay). ANOVA, mean + SEM, n = 6 (***p < 0.0001 for sh-GLT8D1 #1; ***p = 0.0004 for sh-GLT8D1 #2).

Figure 3. *Continued*

(I) Representative images of the migrated GLT8D1-knockdown NCH601 cells after 48h (Boyden chamber assay). Scale bar 100μm.

(J) *GLT8D1* expression in the GLT8D1-knockdown NCH601 cells followed by rescue with the wild type GLT8D1 (qPCR). ANOVA, mean + SEM, n = 4 (*p = 0.0489 for sh-GLT8D1 + *Neo*; *p = 0.0418 for sh-GLT8D1 + rescue).

(K) Quantitative analysis of the cell migration in the GLT8D1-knockdown NCH601 cells followed by rescue with the wild type GLT8D1 after 48h (Boyden chamber assay). ANOVA, mean + SEM, n = 7 (***p = 0.0006 for sh-GLT8D1 + *Neo*; *p = 0.0172 for sh-GLT8D1 + rescue).

(L) Representative images of the migrated GLT8D1-knockdown NCH601 cells or rescue NCH601 cells after 48h (Boyden chamber assay). Scale bar 100μm.

See also Figures S2 and S3.

and 171-DSA-173 (mAS2) (Figure 4A). Native, wild type and both mAS1 and mAS2 mutant GLT8D1 proteins showed enzymatic activity in glycosyltransferase assays for both sugar donors offered (UDP-galactose and UDP-glucose) (Figures 4B and 4C). The average of three independent experiments clearly showed reduced glycosyltransferase activity of mAS1 and mAS2 mutants compared to wild type GLT8D1, with the mAS2 mutant displaying the lowest enzymatic activity on both substrates. When transduced into the GLT8D1-knockdown NCH601 cells, mAS1 and mAS2 showed stable expression levels (Figure S3L). Migration analysis of the GLT8D1-knockdown NCH601 cells in which the mutant proteins were introduced revealed that a stronger reduction of enzymatic activity (mAS2) might be necessary to abort the restoration of pro-migratory properties (Figures 3D, 3E, S3M, and S3N). A third truncated protein lacking the transmembrane domain - ΔTM - was designed (Figure S4A). ΔTM-GLT8D1 showed normal enzymatic activity for both tested donor substrates (UDP-galactose and UDP-glucose), compared with those of wild type GLT8D1 (Figures S4B and S4C). Ectopic expression of the TM-lacking protein in the GLT8D1-knockdown NCH601 cells fully restored their migration capacity (data not shown).

Altogether, these findings indicate that sufficient enzymatic activity, but not the membrane association of GLT8D1 is necessary to mediate its pro-migratory effect.

DISCUSSION

Glioma cell migration and invasion from the tumor core into adjacent brain parenchyma is still one of the key detrimental features in high-grade glioma and especially in glioblastoma. Infiltrative tumor cells often escape both the surgical resection and irradiation interventions, resulting in rapid tumor recurrence. The process of glycosylation has barely been investigated in GBM pathology research, even though there is increasing evidence that aberrant glycosylation represents a cancer hallmark in both peripheral and brain tumors (Lemjabbar-Alaoui et al., 2015; Veillon et al., 2018). Glycosylation is the most abundant posttranslational modification and can be essential for the correct folding, activity, and stability of many proteins (Pinho and Reis, 2015; Rowe and Burkhart, 2018). The glycosyltransferase GLT8D1 has not yet been associated with brain tumor development so far. We showed a significant elevation of *GLT8D1* mRNA expression in human GBM samples as compared to healthy brain tissue (Figure 1D). Kaplan-Mayer analysis in one large cohort of the Cancer Genome Atlas (TCGA) GBM database pointed toward a better survival prognosis for patients with lower *GLT8D1* expression (Figures 1B and 1C). Starting with this observation, the presente study provides for the first time deeper insights into the molecular biological properties of GLT8D1 in GBM. With the help of sequence/conservation analyses of GLT8D1's closest homologs and the available crystal structures of human glycogenin 1 (GYG1) and mouse xyloside xylosyltransferase 1 (XXYLT1), we created a potential 3D protein structure model of GLT8D1 (Figures S1, 2 and Table 1).

In vitro experiments in two different spheres-forming human GBM lines revealed that high *GLT8D1* levels promoted tumor cell migration, whereas its knockdown abolished cell motility (Figures 3D–3L). Although no direct association of GLT8D1 with migration/invasion processes has been shown before, several studies indicated a "motor" phenotype could be caused by diminished enzymatic function of the respective protein. Cooper-Knock et al. identified several mutations in *GLT8D1* that cluster closely to a potential substrate binding site within exon four resulting in impaired GLT8D1 enzymatic activity *in vitro* (Cooper-Knock et al., 2019). These mutations caused motor neuron deficits and co-segregated with ALS disorder. Further investigations by Moll et al. found an association of impaired GLT8D1 enzymatic activity with reduced membrane expression of glycosphingolipids and hence disruption of ganglioside signaling within the CNS (Moll et al., 2019). With regard to tumor development, it has been shown that *GLT8D1* expression levels are significantly enhanced in highly invasive/metastatic tumors e.g., in human cutaneous and mucosal melanoma samples as well as in the head and neck squamous cell carcinomas (HNSCCs) (Hwang et al., 2013; Hu et al., 2019). Moreover, *GLT8D1* expression levels gradually increased from stage I to stage III implying that it could be a marker of poor prognosis in melanoma (Hu et al., 2019).

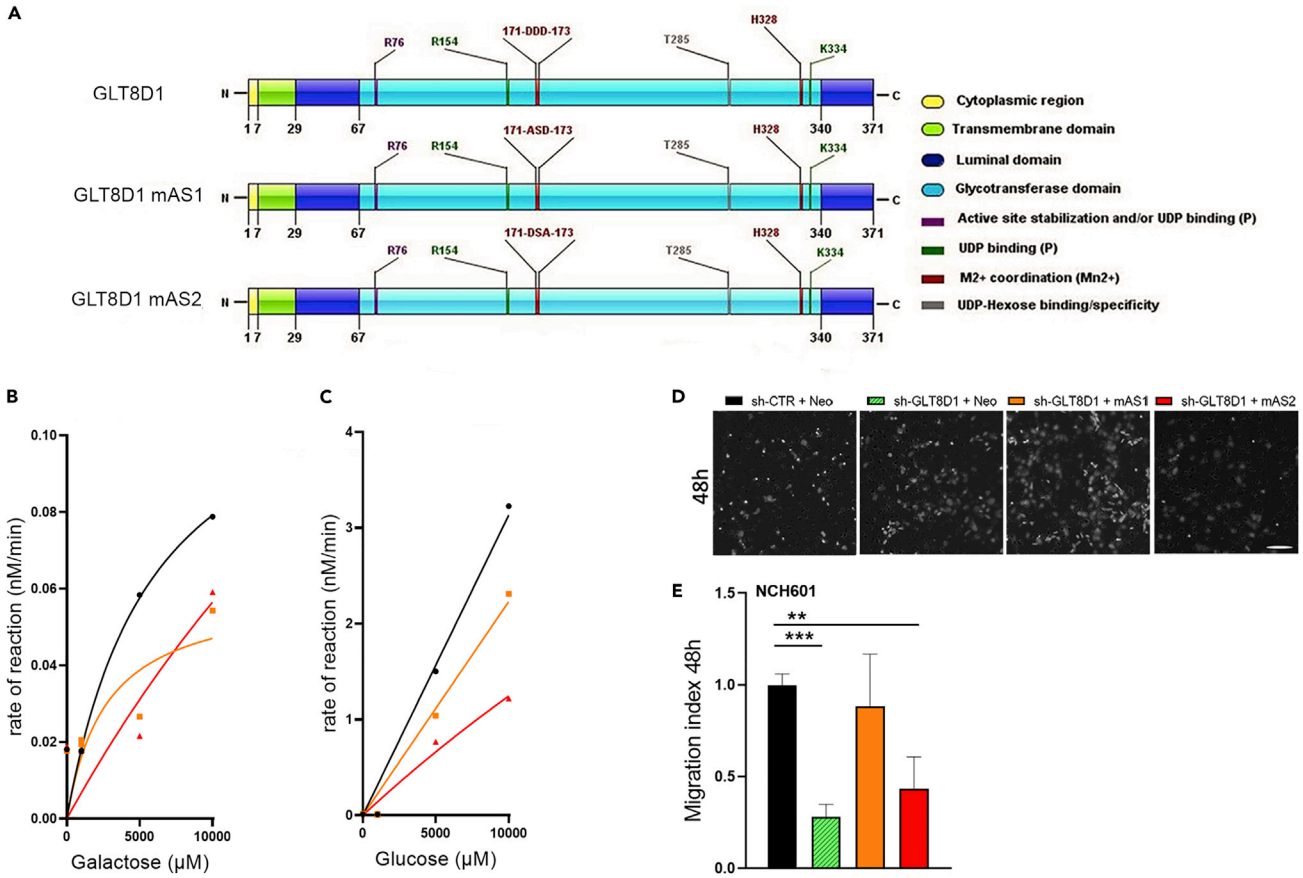

Figure 4. Glycosyltransferase activity of GLT8D1 and its impact on GBM cell migration

(A) Domain organization and mutations in GLT8D1 proteins illustrated using DOG 2.0 software (Ren et al., 2009).

(B) Graph representing glycosyltransferase reaction rate of wild type GLT8D1 (black), mAS1 (orange) and mAS2 (red) using UDP-Galactose as donor substrate (expressed as mean of n = 3).

(C) Graph representing glycosyltransferase reaction rate of wild type GLT8D1, mAS1, and mAS2 (expressed as mean of n = 3) using UDP-Glucose as donor substrate.

(D) Representative images of the migrated GLT8D1-knockdown NCH601 cells followed by rescue with GLT8D1, carrying mutations in the active site (mAS1 or mAS2) after 48h (Boyden chamber assay).

(E) Quantitative analysis of the cell migration in the GLT8D1-knockdown NCH601 cells followed by rescue with GLT8D1, carrying mutations in the active site (mAS1 or mAS2) after 48h (Boyden chamber assay). ANOVA, mean + SEM, n = 5 (***p < 0.0001 for sh-GLT8D1 + *Neo*; **p = 0.0065 for sh-GLT8D1 + mAS2). See also Figure S4.

The *in vitro* study from Yang et al. showed that GLT8D1 knockdown in mouse E14.5 neural stem cells (NSCs) increased their proliferation as well as stem cell marker gene expression indicating that *GLT8D1* has an important function in regulating proliferation and stemness of NSCs (Yang et al., 2018). In contrast to these findings, we did not observe any changes in GBM cell proliferation that could be related to *GLT8D1* expression (Figures S3D, S3H, and S3K).

In line with the observations of Cooper-Knock et al., GLT8D1 was located in both GA and ER compartments in GBM cells (Figures 3C and S2A). This localization pattern and the structural analysis imply that GLT8D1 is enzymatically active. We showed that the pro-migratory effects of GLT8D1 in GBM cells are strongly linked to this glycosyltransferase function (located within its LU domain). Xylose as a putative substrate of GLT8D1 has previously been excluded in the study by Sethi et al., 2010. Cooper-Knock et al. showed galactose-transferring activity *in vitro* and Taujale et al. predicted glucose as a putative substrate of GLT8D1 *in silico* (Cooper-Knock et al., 2019; Taujale et al., 2020). In our study, GLT8D1 showed glycosyltransferase activity with both UDP-galactose and UDP -glucose, the latter being the preferred donor substrate under *in vitro* conditions (Figures 4B and 4C). The generated loss-of-function GLT8D1 mutants mAS1 and mAS2 showed reduced enzymatic activity toward both substrates (Figures 4B and 4C). Generally, the mAS2 mutations

resulted in the lowest enzymatic activity. Interestingly, reduction of the enzymatic activity down to the levels of mAS2 was necessary to abolish the restoration of the pro-migratory effects when the mutants were introduced into the GLT8D1-knockdown GBM cells (Figures 4D and 4E).

LC-MS/MS based analysis of GLT8D1 interactome followed by GO enrichment analysis revealed interaction partners separating into several groups: (i) extracellular exosome proteins, (ii) focal adhesion proteins, and (iii) vesicle proteins (Figures S5A and S5B; Table S3). Among these, several lysosomal-associated and cytoskeleton-associated proteins may be of great interest for further research. Vinculin (Table S3) is known to contribute to the regulation of migration in numerous cancer entities, is able to induce pro-migratory signaling (e.g., PI3K) and localizes to the invasion border of mammal carcinoma (Rubashkin et al., 2015). Loss of vinculin is reported to be associated with adhesion and thus to promote invasion/metastasis in colorectal carcinoma (Li et al., 2014). Interestingly, the major mechanism of vinculin activation comprises phosphorylation (Zhang et al., 2004; Auernheimer et al., 2015), and it has been described, that glycosylation may compete with phosphorylation, hence acting as a PTM switcher of a substrate function (Singh et al., 2015). Another interaction partner, the lysosomal protein cathepsin D – *CTSD* (Table S3) was previously implicated in regulation of invasion in various cancers, including glioma (Benes et al., 2008; Liu et al., 2012). Liu et al. reported that inhibition of lysosome exocytosis negatively regulated tumor cell migration in GBM.

Although we can already propose several potential GLT8D1 interaction partners, further deeper interactome analysis will be necessary to identify the physiological sugar donors and acceptors mediating the pro-migratory effects of GLT8D1. In conclusion, our findings unequivocally corroborate the pro-migratory function of GLT8D1 in glioma that is linked to its enzymatic activity and associated with impaired patient survival. These findings shed light on a distinct pathological function of GLT8D1 in the CNS and thus may provide a new starting point toward novel potential therapeutic targets in GBM treatment.

Limitations of the study

The current study primarily focuses on *in vitro* and *in silico* characterization of the GLT8D1 to decipher its function in GBM pathology. The translational aspect of the study is limited to a semiquantitative analysis of a limited number of patient samples as well as screening of the available databases. The major obstacle at this point is only a restricted availability of the antibodies and a high qualitative variability between different lots of the same antibody. This issue might be solved when more attention is drawn toward the pathological role of GLT8D1 in the CNS, and hence, more commercial interest geared toward improving antibody quality. In addition, although we were able to give the first insights into possible mechanisms behind the pathological role of GLT8D1 (e.g., involvement of its enzymatic activity and interaction with exosomal, cytoskeletal, and vesicle transport proteins) the ultimate regulation of other proteins by GLT8D1 remains to be determined. In our study, GLT8D1 was detected in both ER and GA, and in both these compartments glycosylation may take place as PTM. Although a potential competition between phosphorylation and glycosylation processes has been introduced as one of the discussion points, it is unknown if this is applicable to GLT8D1, and if yes, how it is orchestrated between the compartments within the cell.

STAR★METHODS

Detailed methods are provided in the online version of this paper and include the following:

- KEY RESOURCES TABLE
- RESOURCE AVAILABILITY
  - Lead contact
  - Materials availability
  - Data and code availability
- EXPERIMENTAL MODEL AND SUBJECT DETAILS
  - Cell lines and cell culture conditions
- METHOD DETAILS
  - GLT8D1 expression and Kaplan-Meier analysis using GlioVis platform
  - Comprehensive analysis of GLT8D1 and protein structure 3D-model
  - Overexpression and shRNA-mediated knockdown of GLT8D1
  - Human tissue samples
  - Total RNA isolation and quality control
  - Real-time quantitative PCR

SUPPLEMENTAL INFORMATION

Supplemental information can be found online at https://doi.org/10.1016/j.isci.2022.103842.

ACKNOWLEDGMENTS

M.M. would like to thank the Luxembourg National Research Fond (FNR) for the support (FNR PEARL P16/BM/11192868 grant). The authors would like to thank Prof. Christel Herold-Mende (Experimental Neurosurgery, University Hospital Heidelberg, Germany) for providing glioma cells for this study.

AUTHOR CONTRIBUTIONS

Conceptualization, E.I.I., D.L.G., A.G., G.D., S.P.N., T.M., and M.M.; Methodology, D.L.G., A.S., A.G., G.D., S.P.N., and T.M.; Validation, E.I.I., C.C., M.D.G.E., and T.M.; Formal Analysis, E.I.I., C.C., D.L.G., M.D.G.E., C.J., M-L.T., A.L., V.P., F.B., A.M., M.D., J-J.G., G.D., and T.M.; Investigation, E.I.I., C.C., M.D.G-E., C.J., M-L.T., A.L., V.P., F.B., A.M., A.S., M.D., J-J.G., and T.M.; Writing – Original Draft, E.I.I., D.L.G., and T.M.; Visualization, E.I.I, C.C., D.L.G., M.D.G-E., G.D., S.P.N., and T.M.; Supervision, E.I.I., D.L.G., G.D., S.P.N., T.M., and M.M.; Project Administration, E.I.I., C.C., T.M., and M.M.; Writing – Review & Editing, C.C., D.L.G., M.D.G-E., C.J., M-L.T., A.L., V.P., F.B., A.M., A.S., M.D., A.G., J-J.G., G.D., S.P.N., T.M., and M.M.; Data Curation, D.L-G. and G.D.; Funding Acquisition, M.M.

DECLARATION OF INTERESTS

The authors declare no competing interests.

Received: June 1, 2021
Revised: August 27, 2021
Accepted: January 27, 2022
Published: February 18, 2022

SUPPORTING CITATIONS

The following references appear in the supplemental information: Berman et al., 2000; Chen et al., 2006; Dereeper et al., 2008; Guindon et al., 2010; Larkin et al., 2007; Okonechnikov et al., 2012; Pettersen et al., 2004; Stelzer et al., 2016; Waterhouse et al., 2009, 2018; Zahn-Zabal et al., 2020; Zimmermann et al., 2018.

REFERENCES

Abdul Rahim, S.A., Dirkse, A., Oudin, A., Schuster, A., Bohler, J., Barthelemy, V., Müller, A., Vallar, L., Janji, B., Golebiewska, A., and Niclou, S.P. (2017). Regulation of hypoxia-induced autophagy in glioblastoma involves ATG9A. Br. J. Cancer *117*, 813–825. https://doi.org/10.1038/bjc.2017.263.

Auernheimer, V., Lautscham, L.A., Leidenberger, M., Friedrich, O., Kappes, B., Fabry, B., and Goldmann, W.H. (2015). Vinculin phosphorylation at residues Y100 and Y1065 is required for cellular force transmission. J. Cell Sci. *128*, 3435–3a443. https://doi.org/10.1242/jcs.172031.

Benes, P., Vetvicka, V., and Fusek, M. (2008). Cathepsin D – many functions of one aspartic protease. Crit. Rev. Oncol. Hematol. *68*, 12–28. https://doi.org/10.1016/j.critrevonc.2008.02.008.

Berman, H.M., Westbrook, J., Feng, Z., Gilliland, G., Bhat, T.N., Weissig, H., Shindyalov, I.N., and Bourne, P.E. (2000). The protein Data Bank. Nucleic Acids Res. *28*, 235–242. https://doi.org/10.1093/nar/28.1.235.

Bougnaud, S., Golebiewska, A., Oudin, A., Keunen, O., Harter, P.N., Mäder, L., Azuaje, F., Fritah, S., Stieber, D., Kaoma, T., et al. (2016). Molecular crosstalk between tumour and brain

parenchyma instructs histopathological features in glioblastoma. Oncotarget *7*, 31955–31971. https://doi.org/10.18632/oncotarget.7454.

Bowman, R.L., Wang, Q., Carro, A., Verhaak, R.G.W., and Squatrito, M. (2017). GlioVis data portal for visualization and analysis of brain tumor expression datasets. Neuro Oncol. *19*, 139–141. https://doi.org/10.1093/neuonc/now247.

Brenner, D., and Weishaupt, J.H. (2019). Update on amyotropic lateral sclerosis genetics. Curr. Opin. Neurol. *32*, 735–739. https://doi.org/10.1186/1750-1326-8-28.

Campos, B., Wan, F., Farhad, M., Ernst, A., Zeppernick, F., Tagscherer, K.E., Ahmadi, R., Lohr, J., Dictus, C., Gdynia, G., et al. (2010). Differentiation therapy exerts antitumor effects on stem-like glioma cells. Clin. Cancer Res. *16*, 2715–2728. https://doi.org/10.1158/1078-0432.CCR-09-1800.

Cantarel, B.L., Coutinho, P.M., Rancurel, C., Bernard, T., Lombard, V., and Henrissat, B. (2009). The Carbohydrate-Active EnZymes database (CAZy): an expert resource for glycogenomics. Nucleic Acids Res. *37*, D233–D238. https://doi.org/10.1093/nar/gkn663.

Chaikuad, A., Froese, D.S., Berridge, G., von Delft, F., Oppermann, U., and Yue, W.W. (2011). Conformational plasticity of glycogenin and its maltosaccharide substrate during glycogen biosynthesis. Proc. Natl. Acad. Sci. USA *108*, 21028–21033. https://doi.org/10.1073/pnas.1113921108.

Chen, F., Mackey, A.J., Stoeckert, C.J., Jr., and Roos, D.S. (2006). OrthoMCL-DB: querying a comprehensive multi-species collection of ortholog groups. Nucleic Acids Res. *34*, D363–D368. https://doi.org/10.1093/nar/gkj123.

Cooper-Knock, J., Moll, T., Ramesh, T., Castelli, L., Beer, A., Robins, H., Fox, I., Niedermoser, I., van Damme, P., Moisse, M., et al. (2019). Mutations in the glycosyltransferase domain of GLT8D1 are associated with familial amyothrophic lateral sclerosis. Cell Rep. *26*, 2298–2306. https://doi.org/10.1016/j.celrep.2019.02.006.

Cox, J., and Mann, M. (2008). MaxQuant enables high peptide identification rates individualized p.p.b.-range mass accuracies and proteome-wide protein quantification. Nat. Biotechnol. *26*, 1367–1372. https://doi.org/10.1038/nbt.1511.

Cox, J., Neuhauser, N., Michalski, A., Scheltema, R.A., Olsen, J.V., and Mann, M. (2011). Andromeda: a peptide search engine integrated into the MaxQuant environment. J. Proteome Res. *10*, 1794–1805. https://doi.org/10.1021/pr101065j.

Crowe, A.R., and Yue, W. (2019). Semi-quantitative determination of protein expression UsingImmunohistochemistry staining and analysis: an integrated protocol. Bio Protoc. *9*, e3465. https://doi.org/10.21769/BioProtoc.3465.

Dereeper, A., Guignon, V., Blanc, G., Audic, S., Buffet, S., Chevenet, F., Dufayard, J.F., Guindon, S., Lefort, V., Lescot, M., et al. (2008). Phylogeny.fr: robust phylogenetic analysis for the non-specialist. Nucleic Acids Res. *36*, W465–W469. https://doi.org/10.1093/nar/gkn180.

Devraj, K., Poznanovic, S., Spahn, C., Schwall, G., Harter, P.N., Mittelbronn, M., Antoniello, K., Paganetti, P., Muhs, A., Heilemann, M., et al. (2016). BACE-1 is expressed in the blood–brain barrier endothelium and is upregulated in a murine model of Alzheimer's disease. J. Cereb. Blood Flow Metab. *36*, 1281–1294. https://doi.org/10.1177/0271678X15606463.

Guindon, S., Dufayard, J.F., Lefort, V., Anisimova, M., Hordijk, W., and Gascuel, O. (2010). New algorithms and methods to estimate maximum-likelihood phylogenies: assessing the performance of PhyML 3.0. Syst. Biol. *59*, 307–321. https://doi.org/10.1093/sysbio/syq010.

Hu, H., Li, Z., Zhou, Y., Zhang, Y., Zhao, L., Zhao, W., Huang, Y., and Song, X. (2019). GLT8D1 overexpression as a novel prognostic biomarker in human cutaneous melanoma. Melanoma Res. *29*, 612–620. https://doi.org/10.1097/CMR.0000000000000631.

Hughes, C.S., Foehr, S., Garfield, D.A., Furlong, E.E., Steinmetz, L.M., and Krijgsveld, J. (2014). Ultrasensitive proteome analysis using paramagnetic bead technology. Mol. Syst. Biol. *10*, 757. https://doi.org/10.15252/msb.20145625.

Hwang, S., Mahadevan, S., Qadir, F., Hutchison, I.L., Costea, D.E., Neppelberg, E., Liavaag, P.G., Waseem, A., and The, M.T. (2013). Identification of FOXM1-induced epigenetic markers for head and neck squamous cell carcinomas. Cancer *119*, 4249–4258. https://doi.org/10.1002/cncr.28354.

Larkin, M.A., Blackshields, G., Brown, N.P., Chenna, R., McGettigan, P.A., McWilliam, H., Valentin, F., Wallace, I.M., Wilm, A., Lopez, R., et al. (2007). Clustal W and clustal X version 2.0. Bioinformatics *23*, 2947–2948. https://doi.org/10.1093/bioinformatics/btm404.

Lemjabbar-Alaoui, H., McKinney, A., Yang, Y.W., Tran, V.M., and Phillips, J.J. (2015). Glycosylation alterations in lung and brain cancer. Adv. Cancer Res. *126*, 305–344. https://doi.org/10.1016/bs.acr.2014.11.007.

Li, T., Guo, H., Song, Y., Zhao, X., Shi, Y., Hu, S., Nie, Y., Fan, D., and Wu, K. (2014). Loss of vinculin and membrane-bound β-catenin promotes metastasis and predicts poor prognosis in colorectal cancer. Mol. Cancer *13*, 263. https://doi.org/10.1186/1476-4598-13-263.

Liu, Y., Zhou, Y., and Zhu, K. (2012). Inhibition of glioma cell lysosome exocytosis inhibits glioma invasion. PLoS One *7*, e45910. https://doi.org/10.1371/journal.pone.0045910.

Louis, D.N., Ohgaki, H., Wrestler, O.D., Cavenee, W.K., Ellison, D.W., Figarella-Branger, D., Perry, A., Reifenberger, G., and von Deimling, A. (2016). Chapter 1: Diffuse astrocytic and oligodendrogial tumours. WHO Classification of Tumors of the Central Nervous System, 4th edn (Lyon: International agency for research on cancer), pp. 16–77.

Moll, T., Shaw, P.J., and Cooper-Knock, J. (2019). Disrupted glycosylation of lipids and proteins is a cause of neurodegeneration. Brain *143*, 1332–1340. https://doi.org/10.1093/brain/awz358.

Okonechnikov, K., Golosova, O., and Fursov, M.; UGENE team (2012). Unipro UGENE: a unified bioinformatics toolkit. Bioinformatics *28*, 1166–1167. https://doi.org/10.1093/bioinformatics/bts091.

Pettersen, E.F., Goddard, T.D., Huang, C.C., Couch, G.S., Greenblatt, D.M., Meng, E.C., and Ferrin, T.E. (2004). UCSF Chimera–a visualization system for exploratory research and analysis. J. Comput. Chem. *25*, 1605–1612. https://doi.org/10.1002/jcc.20084.

Pinho, S., and Reis, C. (2015). Glycosylation in cancer: mechanisms and clinical implications. Nat. Rev. Cancer *15*, 540–555. https://doi.org/10.1038/nrc3982.

Pomaznoy, M., Ha, B., and Peters, B. (2018). GOnet: a tool for interactive Gene Ontology analysis. BMC Bioinformatics *19*, 470. https://doi.org/10.1186/s12859-018-2533-3.

Ren, J., Wen, L., Gao, X., Jin, C., Xue, Y., and Yao, X. (2009). DOG 1.0: illustrator of protein domain structures. Cell Res. *19*, 271–273. https://doi.org/10.1038/cr.2009.6.

Rowe, L., and Burkhart, G. (2018). Analyzing protein glycosylation using UHPLC: a review. Bioanalysis *10*, 1691–1703. https://doi.org/10.4155/bio-2018-0156.

Rubashkin, M.G., Cassereau, L., Bainer, R., DuFort, C.C., Yui, Y., u, G., Paszek, M.J., Davidson, M.W., Chen, Y.Y., and Weaver, V.M. (2015). Force engages vinculin and promotes tumor progression by enhancing PI3-kinase activation of phosphatidylinositol (3, 4, 5)-triphosphate. Cancer Res. *74*, 4597–4611. https://doi.org/10.1158/0008-5472.CAN-13-3698.

Sanzey, M., Abdul Rahim, S.A., Oudin, A., Dirkse, A., Kaoma, T., Vallar, L., Herold-Mende, C., Bjerkvig, R., Golebiewska, A., and Niclou, S.P. (2015). Comprehensive analysis of glycolytic enzymes as therapeutic targets in the treatment of glioblastoma. PLoS One *10*, e0123544. https://doi.org/10.1371/journal.pone.0123544.

Sasayama, D., Hori, H., Yamamoto, N., Nakamura, S., Teraishi, T., Tatsumi, M., Hattori, K., Ota, M., Higuchi, T., and Kunugi, H. (2014). ITIH3 polymorphism may confer susceptibility to psychiatric disorders by altering the expression levels of GLT8D1. J. Psychiatr. Res. *50*, 79–83. https://doi.org/10.1016/j.jpsychires.2013.12.002.

Schneider, C., Rasband, W., and Eliceiri, K. (2012). NIH Image to ImageJ: 25 years of image analysis. Nat. Methods *9*, 671–675. https://doi.org/10.1038/nmeth.2089.

Sethi, M.K., Buettner, F.F.R., Krylov, V.B., Takeuchi, H., Nifantiev, N.E., Haltiwanger, R.S., Gerardy-Schahn, R., and Bakker, H. (2010). Identification of glycosyltransferase 8 family members as xylosyltransferases acting on O-glycosylated notch epidermal growth factor repeats. J. Biol. Chem. *285*, 1582–1586. https://doi.org/10.1074/jbc.C109.065409.

Seznec, J., Silkenstedt, B., and Naumann, U. (2011). Therapeutic effects of the Sp1 inhibitor mithramycin A in glioblastoma. J. Neurooncol. *101*, 365–377. https://doi.org/10.1007/s11060-010-0266-x.

Singh, J.P., Zhang, K., Wu, J., and Yang, X. (2015). O-GlcNAc signaling in cancer metabolism and epigenetics. Cancer Lett. *356* (2 Pt A), 244–250. https://doi.org/10.1016/j.canlet.2014.04.014.

Stelzer, G., Rosen, R., Plaschkes, I., Zimmerman, S., Twik, M., Fishilevich, S., Iny Stein, T., Nudel, R., Lieder, I., Mazor, Y., et al. (2016). The GeneCards suite: from gene data mining to disease Genome sequence analysis. Curr. Protoc. Bioinformatics *54*, 1.30.1–1.30.33. https://doi.org/10.1002/cpbi.5.

Taujale, R., Venkat, A., Huang, L.-C., Zhou, Z., Yeung, W., Rasheed, K.M., Li, S., Edison, A.S., Moremen, K.W., and Kannan, N. (2020). Deep evolutionary analysis reveals the design principles of fold A glycosyltransferases. Elife *9*, e54532. https://doi.org/10.7554/eLife.54532.

Vajaria, B.N., Patel, K.A., and Patel, P.S. (2018). Role of aberrant glycosylation enzymes in oral cancer progression. J. Cancirog. *17*, 5. https://doi.org/10.4103/jcar.JCar_7_18.

Veillon, L., Fakih, C., Abou-El-Hassan, H., Kobeissy, F., and Mechref, Y. (2018). Glycosylation changes in brain cancer. ACS Chem. Neurosci. *9*, 51–72. https://doi.org/10.1021/acschemneuro.7b00271.

Vollmann-Zwerenz, A., Leidgens, V., Feliciello, G., Klein, C.A., and Hau, P. (2020). Tumor cell invasion in glioblastoma. Int. J. Mol. Sci. *21*, E1932. https://doi.org/10.3390/ijms21061932.

Waterhouse, A.M., Procter, J.B., Martin, D.M.A., Clamp, M., and Barton, G.J. (2009). Jalview Version 2 – a multiple sequence alignment editor and analysis workbench. Bioinformatics *25*, 1189–1191. https://doi.org/10.1093/bioinformatics/btp033.

Waterhouse, A., Bertoni, M., Bienert, S., Studer, G., Tauriello, G., Gumienny, R., Heer, F.T., de Beer, T.A.P., Rempfer, C., Bordoli, L., et al. (2018). SWISS-MODEL: homology modelling of protein structures and complexes. Nucleic Acids Res. *46*, W296–W303. https://doi.org/10.1093/nar/gky427.

Yang, C.P., Li, X., Wu, Y., Shen, Q., Zeng, Y., Xiong, Q., Wei, M., Chen, C., Liu, J., Huo, Y., et al. (2018). Comprehensive integrative analyses identify GLT8D1 and CSNK2B as schizophrenia risk genes. Nat. Commun. *9*, 838. https://doi.org/10.1038/s41467-018-03247-3.

Yu, H., Takeuchi, M., LeBarron, J., Kantharia, J., London, E., Bakker, H., Haltiwanger, R.S., Li, H., and Takeuchi, H. (2015). Notch-modifying xylosyltransferase-substrate complexes support an SNi-like retaining mechanism. Nat. Chem. Biol. *11*, 847–854. https://doi.org/10.1038/nchembio.1927.

Zahn-Zabal, M., Michel, P.A., Gateau, A., Nikitin, F., Schaeffer, M., Audot, E., Gaudet, P., Duek Roggli, P., Teixeira, D., Rech de Laval, V., et al. (2020). The neXtProt knowledgebase in 2020: data, tools and usability improvements. Nucleic Acids Res. *48*, D328–D334. https://doi.org/10.1093/nar/gkz995.

Zhang, Z., Izaguirre, G., Lin, S.-Y., Lee, H.Y., Schaefer, E., and Haimovich, B. (2004). The phosphorylation of vinculin on Tyrosine residues 100 and 1065, mediated by SRC kinase, affects cell spreading. Mol. Biol. Cell *15*, 4234–4247. https://doi.org/10.1091/mbc.e04-03-0264.

Zimmermann, L., Stephens, A., Nam, S.Z., Rau, D., Kübler, J., Lozajic, M., Gabler, F., Söding, J., Lupas, A.N., and Alva, V. (2018). A completely reimplemented MPI bioinformatics toolkit with a new HHpred server at its core. J. Mol. Biol. *430*, 2237–2243. https://doi.org/10.1016/j.jmb.2017.12.007.

STAR★METHODS

KEY RESOURCES TABLE

REAGENT or RESOURCE	SOURCE	IDENTIFIER
Antibodies		
Rabbit polyclonal anti GLT8D1	Thermo Scientific	Cat# PA5-49000; RRID: AB_2634456
Rabbit polyclonal anti GAPDH	CST	Cat# 5174S; RRID: AB_10622025
Mouse monoclonal anti HA	Sigma	Cat# H9658; RRID: AB_260092
Rabbit polyclonal anti LaminB1	Abcam	Cat# ab16048; RRID: AB_443298
Mouse monoclonal anti mitochondria (MTC02)	Abcam	Cat# ab3298; RRID: AB_303683
Rabbit polyclonal anti GLUT1	Abcam	Cat# ab652; RRID: AB_305540
Mouse monoclonal anti EEA1	Novus Biologicals	Cat# MAB8047
Mouse monoclonal anti PDI	Enzo	Cat# SPA-891; RRID: AB_10615355
Mouse monoclonal anti Golgin97	CST	Cat# 97537S; RRID: AB_2800280
Mouse monoclonal anti LAMP1	CST	Cat# 15665S; RRID: AB_2798750
Biological samples		
Normal appearing human brain samples	University Hospital Frankfurt am Main, Germany	N/A
Human glioblastoma (WHO grade IV) samples	University Hospital Frankfurt am Main, Germany	N/A
Critical commercial assays		
Duolink Proximity Ligation Assay	Merck	DUO92101
UDP-GloTM Glycosyltransferase Assay	Promega	V6961
Deposited data		
GLT8D1 interactome dataset	PRIDE repository	PRIDE: PXD027854
Experimental models: cell lines		
Human primary stem-like glioblastoma cell line NCH644	Christel Herold-Mende	https://doi.org/10.1002/path.4366
Human primary stem-like glioblastoma cell line NCH601	Christel Herold-Mende	https://doi.org/10.1002/path.4366
Oligonucleotides		
Primers for the generation of mutation constructs, see Table S1	This paper	N/A
Primers for qPCR, see Table S2	This paper	N/A
Recombinant DNA		
pcDNA3.1 + C-HA	GeneScript	N/A
pGIPZ GLT8D1 shRNA #1 and #2	Open Biosystem	V3LHS-329046, V3LHS-403938
Non-silencing-GIPZ lentiviral shRNA	Open Biosystem	RHS4346
pCDH-EF1a-IRES-Neo	Systems Bioscience	CD533A-2
pCMVdeltaR8.74	Didier Trono	Addgene plasmid #12263
pMD.G.2	Didier Trono	Addgene plasmid #12259
Software and algorithms		
ImageJ	Schneider et al., 2012	https://doi.org/10.1038/nmeth.2089
Bioinformatic databases used for GLT8D1 structural analysis, see Table S4	This paper	N/A

(*Continued on next page*)

Continued

REAGENT or RESOURCE	SOURCE	IDENTIFIER
GOnet web-application	Pomaznoy et al., 2018	http://tools.dice-database.org/GOnet/
Motifolio	license to Michel Mittelbronn	www.motifolio.com
Other		
GlioVis platform	Bowman et al., 2017	http://gliovis.bioinfo.cnio.es

RESOURCE AVAILABILITY

Lead contact

Further information and requests for resources and reagents should be directed to and will be fulfilled by the lead contact, Prof. Dr. Michel Mittelbronn (michel.mittelbronn@lih.lu).

Materials availability

This study did not generate new unique reagents.

Data and code availability

This paper analyzed existing, publicly available data. The accession numbers for these datasets are listed in the STAR Methods and in the key resources table. The interactome dataset produced in this study has been deposited to the PRIDE repository under project name "Enzymatic activity of glycosyltransferase GLT8D1 promotes human glioblastoma cell migration" and project accession number PRIDE: PXD027854. Specialist data of interest (coordinates in PDB format for the core model of (human) GLT8D1 and access to the interactome dataset) will be provided by the lead contact upon request. This paper does not report any original computer code. Any additional information required to reanalyze the data reported in this paper is available from the lead contact upon request.

EXPERIMENTAL MODEL AND SUBJECT DETAILS

Cell lines and cell culture conditions

Patient-derived glioblastoma stem-like cultures (NCH644 and NCH601) were kindly provided by Dr. Christel Herold-Mende (University of Heidelberg, Germany) and cultured as previously described (Campos et al., 2010; Sanzey et al., 2015). In brief, NCH644 cells were maintained in neurobasal medium (Invitrogen, Carlsbad, California, USA) supplemented with 2% (v/v) ultraglutamine (Lonza, Basel, Switzerland), 1x B27 supplement (Lifetech, Carlsbad, California, USA), 1 U/ml heparin (Sigma Aldrich, St. Louis, Missouri, USA), 100 U/ml penicillin and 0.1 mg/ml streptomycin (Sigma Aldrich), 20 ng/ml epidermal growth factor (EGF) (Provitro, Berlin, Germany) and 20 ng/ml basic fibroblast growth factor (bFGF) (Milteny, Bergisch Gladbach, Germany). NCH601 cells were maintained in DMEM-F12 medium (Lonza) supplemented with 2% (v/v) ultraglutamine, 1x BIT100 supplement (Provitro), 1 U/ml heparin, 100 U/ml penicillin and 0.1 mg/ml streptomycin, 20 ng/ml EGF and 20 ng/ml bFGF. The cells were cultured in a humidified atmosphere at 5% CO_2 and 37 °C and routinely checked for mycoplasma contamination using the MycoAlert mycoplasma detection kit (Lonza). The spheroids morphology was estimated with EVOS fl AMF-4306 AMG microscope (Westburg, Leusden, Netherlands).

METHOD DETAILS

GLT8D1 expression and Kaplan-Meier analysis using GlioVis platform

The mRNA expression of GLT8D1 in glioblastoma- and non-tumor specimen as well as Kaplan-Meier survival analysis on glioblastoma-bearing patients with high- vs. low GLT8D1 expression was performed using the GlioVis platform: http://gliovis.bioinfo.cnio.es (Bowman et al., 2017). The Cancer Genome Atlas (TCGA_GBM) dataset and HG-U133A platform was used (in total 538 entries). Statistical analysis was performed by the platform as following: Tukey's Honest Significant Difference (HSD) was used to analyze mRNA expression and Log-rank and Wilcoxon tests for Kaplan-Meier analysis.

Comprehensive analysis of GLT8D1 and protein structure 3D-model

Our initial analyses and submissions to online-bioinformatics methods in support of structural/functional predictions and modeling as described here were carried out November-December 2018, and repeated in June

2020 to ascertain consistency and report up-to-date scores. A list of substantially contributing resources to these analyses is provided in Table S4 below, with access links and literature references. Coordinates in PDB format for the core model of (human) GLT8D1 are available upon request to the authors. Multiple sequence alignments (MSAs) of GLT8D1 and its closest homologs were derived by uniting and vetting the OrthoMCL groups including GLT8D1 (ENSEMBL: hsap|ENSP00000419612; OrthoMCL: OG5_136216) and its close paralog GLT8D2 (ENSEMBL: hsap_ENSP00000354053; OrthoMCL: OG5_135167) by removing duplicates and potentially erroneous sequences, realigning (ClustalX, UGENE), and finally removing further homologs with insufficiently corroborated orthology to either GLT8D1 or GLT8D2, as verified via consistency with speciation of sequence derived phylogenetic trees (PhyML at Phylogeny.fr, 100 bootstraps, JTT-model, outgroups: GAT-L4_ARATH, A0A103XSY6_CYNCS, 2U4W2_SALR5) (data not shown). While GLT8D2 (encoded on Chromosome 12: 12q23.3) is not functionally relevant to this study because it is not expressed in brain tissues (GTEx: GLT8D2) its close paralogy to GLT8D1 (49% identity at the amino acid (a.a.) level) and structural similarity in the lumenal (LU) domain makes it informative in the context of MSA-based structural prediction. Based on these criteria we worked primarily with the metazoan-only MSA shown in Figure S1 (22 homologous sequences from 13 model species). We note that the actual representation of the two proteins in metazoan model species is richer than is reflected by this alignment. This is because obviously erroneous i.e. mispredicted, protein sequences were removed from the original set of OrthoMCL (ENSEMBL) sequences even if only one exon was affected. For the purpose/conclusions drawn in this research, taxonomic completeness was not required. However, for studies that require appreciation of the evolutionary spectrum of the gene/protein family, corrected putative protein translations should be used to replace the removed sequences (e.g. putative orthologs of GLT8D2 in mouse and rat).

Suitable template structures for modelling were identified through searches with HHpred against its representative subset of the Protein Data Bank (PDB) with <70% mutual sequence identity (PDB_mmCIF70), by submitting GLT8D1 sequence alone or the MSA in segments of the predicted LU domain over which sequence conservation among homologs was obviated in the MSA. Due to the regionally differing degree of conservation/variation that is found in the GT-A fold superfamily (Taujale et al., 2020) and the lack of a very close homolog with determined 3D-structure, HHpred searches returned many GT-A fold structures with high-confidence scores but with inconclusive ranking as one would anticipate in such cases (see below for specific scores and ranks; all submissions to the HHpred server used default parameters except: E-value inclusion threshold = 1E-10; Min. seq. Identity of MSA hits = 10%; Min coverage of MSA hits = 60%; Max number of MSA generation steps: 3 (GLT8D1 alone) or 0 (MSA)). From these HHpred hits we selected on phylogenetic/functional grounds the crystal structures of murine Xyloside xylosyltransferase 1 (XXYLT1; PDB: 4wma, 1.62 Å resolution, Yu et al., 2015) and human Glycogenin-1 (GYG1; PDB: 3qvb, 2.26 Å resolution, Chaikuad et al., 2011) *a priori*.

To produce high-confidence target-template alignments for 3D-modeling, we refined the respective automatically proposed HHpred alignments of each of these potential template structures with the target fragment spanning GL8D1_HUMAN residues 62-354 (HHpred E-value scores 4wma: 1.1E-24 (GLT8D1 alone), 8.4E-17 (MSA), at ranks 9-10; HHpred E-value scores 3qvb: 9.4E-23 (GLT8D1 alone), 2.3E-14 (MSA), at ranks 10-12); this fragment was most compatible with the protein fold and conservation patterns in the GLT8D1 MSA (shown in Figure S1). We performed this refinement with the help of (1) close-homolog MSAs for each template that were produced by subjecting their respective OrthoMCL families to the same process as we applied above to produce the target MSA and described above (data not shown; note that for 3qvb this close-homolog MSA included its close paralog GYG2), and (2) targeted close inspection of the template structures. In combination, (1) and (2) helped us to favor structurally optimized insertion or deletion sites through minor modifications of the gap placement in the original HHpred-proposed alignments that served as starting points for each model-to-template alignment (Figure S1).

Next, coordinates for 3D-models built onto each template structure were produced using SWISSMODEL online, with user-provided alignments and monomeric templates. Although the aligned model-to-template sequence identity may seem quite low to non-experts (18% onto PDB: 3qvb; 14% onto PDB: 4wma), the structural core of the GT-A fold, active site motifs (Taujale et al., 2020) and location of the UDP-hexose pocket in this clade are highly conserved i.e. both structures are suitable templates for GLT8D1 and its close homologs in these particular regions. Based on comparisons of the two resulting models and consistency with other known structures in the GT-A family (visualized/analyzed in UCSF Chimera Software), we selected PDB: 3qvb_A as our final template and replaced GLT8D1 residues

201-237 with a 'GGG' in the final modelling run which was subsequently excised as no confident template fragment was found for this hypervariable region ("HV2" in Taujale et al., 2020).

Expert curation/refinement thus allowed us to produce a coordinate model that we deem equivalent in accuracy to a medium-resolution crystal structure in its backbone and side-chain directionality around the active site (Figures 2A–2C and Table 1; SM: QMEAN = -4.24, Cβ = -2.1). This was further corroborated by: (1) clash-free transference of co-crystallized UDP-Glucose (UDPG) and substrate from PDB: 4wma into the model, and (2) the proximity of C200 and C239 (C_{α} distance = 9.2 Å) because a potential disulfide bond between these strongly conserved cysteine residues would be consistent with this domain's predicted lumenal location (lumenal within the Golgi apparatus as it is first demonstrated in this report) whereas generally intracellular cytoplasmic disulfide bridges are rare.

While mechanistic details for this enzyme are still outstanding, we inferred the importance and roles of some GLT8D1 residues near the putative active site based on the MSA and the 3D-model to be: 'evident' if conservation/consistency extended across several subfamilies of the GT-A fold (Taujale et al., 2020); 'confident' where we postulate a contribution at least across the GLT8D1-GLT8D2 family (Figure S1); or 'predicted' where the amino acid is not common in this role but conservation and location make it highly compelling. We note that meanwhile the machine-learning (ML) predictions of sugar specificity by Taujale et al. using sequence/structure features may point to UDP-Glucose as the favored donor candidate *in vivo* for GLT8D1 glycosyltransferase activity (with moderate prediction confidence, Taujale et al., 2020). While UDP-Glucose would also be compatible with our structural model and predictions, experimental evidence will be required to pin-point the natural donor and substrate/s of GLT8D1; at its current resolution/confidence the model cannot persuasively contribute to shedding light on this question.

Overexpression and shRNA-mediated knockdown of GLT8D1

The *GLT8D1* coding sequence (clone ID: OHu16854C) inserted in pcDNA3.1 + C-HA vector via XhoI and ApaI restriction sites was used to generate the overexpressing vector (GenScript, Piscataway, New Jersey, USA). Knockdown of *GLT8D1* was achieved by two pGIPZ lentiviral shRNAs (clone IDs: V3LHS-329046 and V3LHS-403938, RHS4531-EG55830, Open Biosystems, Huntsville, Alabama, USA), designated as sh-GLT8D1 #1 and #2, respectively, the latter targeting the 3'UTR region of the *GLT8D1* transcript. A non-targeting shRNA (sh-CTR, RHS4346, Open Biosystems) was used as control.

For stable expression, the *GLT8D1-HA* fragment was inserted into empty pCDH-EF1a-IRES-Neo plasmid (#CD533A-2, Systems Biosciences, Palo Alto, California, USA) via XbaI and NotI restriction sites, to generate the "pCDH-EF1a-GLT8D1-HA-IRES-Neo" expression plasmid. Empty vector (later referred to as Neo) was used as a negative control. Additionally, the following expression plasmids with mutated *GLT8D1* were generated: pCDH-EF1a-Neo with the protein product GLT8D1-HA lacking the N-terminal transmembrane domain (ΔTM-GLT8D1-HA, further referred as ΔTM), and with the protein products GLT8D1-HA carrying mutations in the predicted active site involved in the metal ion coordination (GLT8D1-HA D171A/D172S, further referred to as mAS1, GLT8D1-HA D172S/D173A, further referred to as mAS2. The mAS1- and mAS2-expressing plasmids were cloned by overlapping PCR. The ΔTM expressing plasmid was cloned by PCR with introduction of alternative XbaI restriction site and start codon after L33 amino acid. The resulting fragments were inserted into pCDH-EF1a-Neo via XbaI and NotI restriction sites. For information about primers used for cloning see Table S1. For rescue overexpression, pCDH vector alone (Neo) or with *GLT8D1-HA*-construct was introduced into NCH601 cells with either sh-CTR or with sh-GLT8D1 #2.

Lentiviral particles were produced as described previously (Abdul Rahim et al., 2017). In brief, Hek293T cells were co-transfected with pGIPZ or pCDH transfer plasmids together with the viral core packaging construct pCMVdeltaR8.74 (gifted from Didier Trono; Addgene plasmid #12263) and the VSV-G envelope protein vector pMD.G.2 (gifted from Didier Trono; Addgene plasmid #12259) with the help of X-tremeGENE HP DNA transfection reagent (Sigma Aldrich). Supernatant containing viral particles was used to transduce 100,000 cells and G418 selection (3 mg/ml for NCH644 or NCH601, Invivogen, San Diego, California, USA) or puromycin selection (1 mg/ml for NCH601, Sigma-Aldrich) permitted to obtain stably transduced cells.

Human tissue samples

Human glioblastoma, WHO grade IV, and normal-appearing brain specimens were collected at the University Hospital Frankfurt am Main, Germany. The diagnoses were performed by at least two experienced

neuropathologists according to the more recent WHO classification for tumors of the central nervous system (Louis et al., 2016). The use of patient material was approved by the ethical committee of the Goethe University Frankfurt, Germany (GS04/09 and SNO-10-2014). The obtained normal-appearing brain specimen showed no clinical or neuropathological evidence for brain pathology. For RNA extraction cryo-preserved specimens were used. For immunohistochemical stainings, all specimens were fixed in 4% paraformaldehyde (formalin) and paraffin-embedded according to an automated standard protocols.

Total RNA isolation and quality control

Total RNAs were extracted using the TRIzol Lysis reagent (Invitrogen) according to the manufacturers protocol. RNA purity was monitored using NanoDrop® ND-1000 spectrophotometer (Thermo Scientific, Waltham, Massachusetts, USA).

Real-time quantitative PCR

Overall, 1 μg of total RNA was reverse transcribed using iScript cDNA Synthesis Kit (BioRad, Hercules, California). Quantitative PCR (qPCR) was carried out using Fast SYBR Green Master Mix and the Viia 7 Real Time PCR System (Life Technologies). Fold-change (fc) was calculated using the ΔΔCt method using Elongation factor 1-alpha (*EF1α*) as housekeeping gene (see Table S2 for primers and target information).

Protein lysate preparation and subcellular fractionation

Cultured spheroids were lysed in RIPA buffer with Chaps (50 mM, Tris pH 7.5, 150 mM NaCl, 0.1% SDS, 0.5% sodium deoxycholate, 1% NP40, 0.3% Chaps). Protease and phosphatase inhibitor cocktail (Thermo Scientific) were added prior to lysis. Fractionation of cultured spheroids was performed by classic differential centrifugation as previously described (Devraj et al., 2016). In brief, spheroids were lysed in isotonic Hepes-EDTA-Sucrose buffer (HES; 10:1:250 mM, pH 7.4, plus protease and phosphatase inhibitor cocktail) and fractionated using pre-cooled table top centrifuge (5424R, Eppendorf, Hamburg, Germany) and Optima MAX-XP Ultracentrifuge (Beckman Coulter, Brea, California, USA). The following fractions were obtained: total lysate (TL, before fractionation), nuclear pellet (NP, corresponding to centrifugation for 10 min at 1000g), Golgi/mitochondrial pellet (TGN, corresponding to centrifugation for 15 min at 15.000g), plasma membrane pellet (PM, corresponding to centrifugation for 1h at 80.000g), endosomal vesicles (EN, corresponding to centrifugation for 3h at 220.000g) and the residual cytoplasmic proteins (Cyto). Protein concentration was determined by BCA assay (Thermo Scientific).

Western blotting

Overall, 20 μg of proteins were loaded and separated in a NuPAGE Novex 4–12% Bis-Tris Gels (Life Technologies) followed by electroblot transfer to a nitrocellulose membrane (Life Technologies). For fractionated proteins, 20 μg of total lysate and subsequent proportions of the following fractions corresponding to initial protein concentration were separated and blotted in the same way. Membranes were blocked with 1x RotiBlock (Roth, Karlsruhe, Germany) prior to incubation with primary antibodies (rabbit-anti-GLT8D1, Thermo Scientific 1:250; rabbit-anti-glyceraldehyde 3-phosphate dehydrogenase (GAPDH), CST (Danvers, Massachusetts, USA) 1:1000; mouse-anti-HA-tag, Sigma 1:1000; rabbit-anti-Lamin B1, Abcam (Cambridge, United Kingdom) 1:2500; mouse-anti-MTC02, Abcam 1:1000; rabbit-anti-glucose transporter 1 (GLUT1), Abcam 1:750; mouse-anti-early endosome antigen 1 (EEA1), Novus Biologicals (Littleton, Colorado, USA) 1:500). After subsequent incubation with horseradish peroxidase (HRP)-coupled secondary antibodies (Jackson Immuno Research, West Grove, Pennsylvania, USA), chemiluminescent signal was detected by SuperSignal™ West Femto Maximum Sensitivity Substrate (Thermo Scientific) with luminescent image analyzer (Image Quant LAS4000, GE Healthcare, Diegem, Belgium). Quantification was performed with the help of ImageJ by densitometry approach. Pixel densities of studied proteins were normalized to the respective loading controls, and the control condition was set as "1" for a better data presentation.

Proximity ligation assay

To measure the association of GLT8D1 to cellular organelles by protein-protein interaction method, a proximity ligation assay (PLA) was performed with Duolink PLA kit according to the manufacturers protocol (Sigma Aldrich). This method is based on DNA-ligation and amplification of two fluorescently-marked single-stranded complementary oligonucleotides and allows a highly sensitive detection of interacting protein, when the distance between them is below 40 nm. In brief, 10,000 GLT8D1-overexpressing NCH644- or GLT8D1-knockdown NCH601- or rescue cells were seeded on the extracellular matrix (ECM)- (NCH644)

(Sigma Aldrich) or laminin-coated (NCH601) (Thermo Scientific) 8- or 12-well μ-slides (ibidi, Graefeling, Germany), respectively, and let attached overnight. Next day, cells were fixed in 4% paraformaldehyde (PFA), permeabilized and blocked with Duolink blocking solution. Cells were co-stained using two primary antibodies: rabbit-anti-GLT8D1 (Thermo Scientific, 1:50) and one of the following organelle-specific antibodies: mouse-anti-protein disulfide isomerase (PDI) for endoplasmic reticulum (Enzo (Farmingdale, New York, USA), 1:50), mouse-anti-Golgin97 for Golgi apparatus (CST, 1:25), mouse-anti-lysosomal-associated membrane protein 1 (LAMP1) for lysosomes (CST, 1:50), mouse-anti-Catalase for peroxisomes (Novus Biologicals, 1:50) or mouse-anti-MTC02 for mitochondria (Abcam, 1:200). Duolink probes were used as secondary antibodies: Duolink *in situ* PLA probe anti-Rabbit PLUS and Duolink *in situ* PLA probe anti-mouse MINUS. Ligation of the probes was performed by Duolink ligase and signal was amplified by polymerase. Nuclei were stained with Hoechst (Life Technology, 1:1000). The staining protocol without primary antibody was used as a negative control. Stainings were analyzed using LSM880 confocal microscope (Zeiss, Oberkochen, Germany).

Immunohistochemistry (IHC)

Immunohistochemistry was performed on 3μm thick slides from FFPE tissue samples on the automated IHC staining system Dako Omnis (Agilent, Santa Clara, California, USA). The rabbit-anti-GLT8D1 (Thermo Scientific, 1:250) antibody was used. The staining procedure on the Dako Omnis (Agilent) included heat and chemical treatment of the slides with EnVision FLEX TRS, low pH at 97°C for 30 min, incubation with primary antibodies for 20 min and endogenous enzyme block with EnV FLEX Peroxidase-Blocking solution for 3 min. The incubation with EnV Flex + Rabbit LINKER for 10 min was used for signal enhancement. Then, the EnV FLEX/HRP labeled polymer was used as secondary antibody for 20 min, followed by incubation with the DAB (3,3′-Diaminobenzidin)-containing EnVision™ FLEX Substrate working solution for 5 minutes. Slides were counterstained with hematoxylin and mounted with coverslipping film Tissue-Tek (Sakura, Staufen, Germany). Slides were then scanned in the Philips IntelliSite Pathology Solution Ultrafast Scanner 1.6 and analyzed with the Philips IntelliSite Pathology Solution Software.

Cell migration assay

The Boyden chamber migration assay has been described in detail previously (Seznec et al., 2011). In brief, 50,000 cells were seeded on an 8μm membrane (Greiner, Kremsmünster, Austria) and let migrate over 48h. 10% fetal calf serum (FCS) was applied into the lower chamber as a chemoattractant. The migration was analyzed 24h and 48h after start of the experiment by fixing the cells, removing the non-migrating cells, staining the migrated cells with Hoechst and counting the migrated cells on five regions of interest (ROIs) per membrane at the Nikon DS Ri2 microscope (Nikon, Tokyo, Japan) with 10x magnification objective. Two membranes per biological replicate and at least four biological replicates were taken for statistical analysis. Migration index was calculated as fold change (fc) between the control cells versus overexpression, knockdown or rescue cells relative to 1.

Cell proliferation assay

To measure the proliferation of the GLT8D1-overexpressing NCH644- or GLT8D1-knockdown NCH601- or rescue cells, 50,000 cells were seeded on the ECM- (NCH644) (Sigma Aldrich) or laminin-coated (NCH601) (Thermo Scientific) 24-well plates and visualized using automated IncuCyte Live Cell Analysis System (Sartorius, Göttingen, Germany) for 96h with 12h intervals with 10x magnification objective. Cell density was calculated for each time point from at least two ROIs per well. At least three biological replicates with two technical replicates each has been taken for statistical analysis. Proliferation index was calculated as relative to 1 ratio between the control cells versus overexpression, knockdown or rescue cells over 96h.

HA-tag pulldown assay

HA-tag pulldown of the GLT8D1-HA from NCH644-overexpressing vs. control (Neo) cells with interacting proteins was performed with Pierce HA-Tag immunoprecipitation (IP)/Co-IP kit according to the manufacturers protocol (Thermo Scientific). Eluted proteins were subjected to subsequent LC-MS/MS analysis of the GLT8D1 interactome.

Mass spectrometry-based interactomics

The proteins eluted from the anti-HA beads were cleaned up and digested using the single-pot solid phase-enhanced sample preparation (SP3) as described in Hughes et al., 2014. The cleaned-up proteins

were alkylated with iodoacetamide and digested with Trypsin over night at 37 °C. The peptides were recovered from the SP3 beads, acidified with 1% formic acid. Peptides were separated on a 15cm reverse-phase column (Pepmap18, Thermo Scientific) using a gradient to 40% acetonitrile (Merck) Separated peptides were ionized on a Proxeon ion source and directly sprayed into the online-coupled VELOS-OrbiTRAP mass spectrometer (Thermo Scientific). MS1 spectra were recorded with a mass resolution of 60,000 in the orbitrap part of the machine. MS2 spectra were recorded in the VELOS. The ten most intense ions with a charge state greater than 1 were selected (target value = 500; monoisotopic precursor selection enabled) and fragmented in the linear quadrupole trap using CID (collision induced dissociation, 35% normalized collision energy). Dynamic exclusion for selected precursor ions was 60 s. Recorded spectra were analyzed using MaxQuant software package (Cox and Mann, 2008) and the human Uniprot database, allowing for 2 missed cleavages. Fixed modifications were set to cysteine carbamylation, and variable modifications were set to methionine oxidation, as well as N-terminal protein acetylation. Each replicate was analyzed separately with the label-free option activated for data quantification (Cox et al., 2011).

In vitro glycosyltransferase activity assay

Hek293T cells were transfected with pCDH-EF1a-IRES-Neo vectors expressing mutants or wild-type *GLT8D1* fused to an HA-tag using the calcium-phosphate transfection method. 48h after transfection cells were lysed in lysis buffer (150mM NaCl, 1mM EDTA, 1mM DTT, 0.5% Triton X-100, 50mM HEPES, 10% glycerol, pH 7.5). Immunoprecipitation of HA-tagged protein was performed by incubating the lysates with anti-HA magnetic beads (Sigma Aldrich) for 1 hour rotating at 4 °C. HA-tagged protein was eluted in a 1μg/μl HA-peptide in PBS (Sigma Aldrich). Eluted protein concentration was determined using BCA assay (Thermo Scientific). Protein purification was validated by western blot using an antibody against the HA-tag. Glycosyltransferase activity was determined using a UDP-Glo™ Glycosyltransferase Assay kit (Promega, Madison, Wisconsin, USA) according to the manufacturer's instructions. A 10 μL reaction was initiated by adding 10 ng/μl of purified protein to an uridine diphosphat (UDP)-sugar substrate (UDP-galactose (supplied within the kit) or UDP-Glucose (Sigma Aldrich) in 5mM $MnCl_2$ (Merck, Kenilworth, New Jersey, USA) and 1xPBS. Reactions were assembled in 384-well plate and incubated at 37°C for 60 minutes. To determine kinetic parameters of the glycosyltransferase reaction, multiple reactions with varying concentrations (0μM, 100μM, 1000μM, 5000μM, 10000μM) of the respective substrate were carried out simultaneously. The GLT8D1 glycosyltransferase reaction was terminated by adding 10 μL UDP detection reagent to each well followed by the incubation at room temperature for 60 min protected from light. Luminescence was recorded using the Clariostar (BMG Labtech, Ortenberg, Germany). A standard curve of UDP in 5mM $MnCl_2$ and 1xPBS was applied at each measurement to associate a defined UDP concentration with a luminescence signal that directly correlates with the glycosyltransferase activity within 60min under described conditions.

The Glycosyltransferase reaction rate was determined as UDP-substrate turnover in nmol per minute (nmol/min) for respective concentration of substrate input. It is important to notice that the concentration of respective glycosyltransferase was constant set as 100ng each reaction.

QUANTIFICATION AND STATISTICAL ANALYSIS

Semi-quantitative determination of GLT8D1 expression on IHC staining

Analysis of GLT8D1 protein level in IHC stained FFPE tissue samples has been performed according to the publication by (Crowe and Yue, 2019). The raw IHC images (.tiff format) were analyzed using ImageJ Fiji software. The images are splitted in HE and DAB staining using "Image" -> "Color" -> "Color Deconvolution" and the H DAB vector. Minimum threshold on the brownish DAB staining image was set to zero while maximum threshold level was set to remove unspecific background staining. Same threshold values were applied on all IHC images. By measuring the mean grey value the average pixel intensity of the DAB staining per image was determined and expressed relative to the number of nuclei within corresponding image.

GO term enrichment analysis

Proteins interacting with WT GLT8D1 identified by LC-MS/MS were analyzed for an overrepresentation in cellular compartment GO terms using the open-source GOnet web-application, available at http://tools.dice-database.org/GOnet/ (Pomaznoy et al., 2018).

Statistics

The figures show data obtained from at least three independent experiments as indicated in the figure legends. Each independent experiment had at least two technical replicates. Numbers and types of controls are stated for each experiment individually in the figure legends. Statistical analyses were performed using GraphPad Prism version 7.0 (GraphPad, San Diego, California, USA). Quantitative data was assessed for significance by unpaired student's t-test between the control- and the experimental conditions (alpha = 0.05; *$p < 0.05$; **$p < 0.01$; ***$p < 0.001$).